Well-Tempered Metadynamics as a Tool for Characterizing Multi-Component, Crystalline Molecular Machines

Andrew J. Ilott,[*,†,‡] Sebastian Palucha,[†] Paul Hodgkinson,[†] and Mark R. Wilson[†]

Department of Chemistry, University of Durham, South Road, Durham, UK DH1 3LE

E-mail: andrew.ilott@nyu.edu

[*]To whom correspondence should be addressed

[†]Department of Chemistry, University of Durham, South Road, Durham, UK DH1 3LE

[‡]Current address: Chemistry Department, New York University, New York, NY 10003, USA

Abstract

The well-tempered, smoothly converging form of the metadynamics algorithm has been implemented in classical molecular dynamics simulations and used to obtain an estimate of the free energy surface explored by the molecular rotations in the plastic crystal, octafluoronaphthalene. The biased simulations explore the full energy surface extremely efficiently, more than four orders of magnitude faster than unbiased molecular dynamics runs. The metadynamics collective variables used have also been expanded to include the simultaneous orientations of three neighboring octafluoronaphthalene molecules. Analysis of the resultant three-dimensional free energy surface, which is sampled to a very high degree despite its significant complexity, demonstrates that there are strong correlations between the molecular orientations. Although this correlated motion is of limited applicability in terms of exploiting dynamical motion in octafluoronaphthalene, the approach used is extremely well suited to the investigation of the function of crystalline molecular machines.

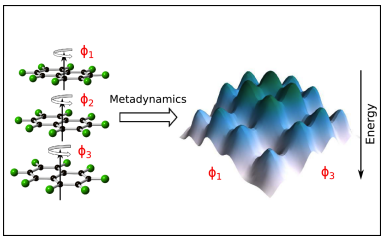

Introduction

In recent years there has been a surge of interest in synthesizing molecules that show promise as components of functional nano machines. Inspired by the complexity and efficiency of highly evolved biomolecular motors such as ATP synthase,[1] flagella,[2,3] and other motor proteins, such as those found in muscle tissue,[4] chemists have designed molecular components resembling molecular gears,[5] turnstiles,[6] gyroscopes,[7] compasses,[8] switches,[9] shuttles,[10] and even more complicated components such as molecular motors[11,12] and various types of 'nanovehicle'.[13] The overall goal of these systems is identical to that of their macroscopic and biological analogues: to react to some

external stimulus; mechanical, chemical, or optical, and produce a coherent mechanical response that results in some useful work being performed. Of particular interest to the study described here is the class of crystalline molecular machines,[14,15] which are rigid systems of individual functional molecules that can either interact with one another in a well-defined way, much like a conventional machine, or act collectively to affect the macroscopic properties of the bulk. Examples of the latter have already been demonstrated in the liquid crystal phase, where properties of the constituent molecules have been modified to react to external stimuli, changing bulk properties such as the color[16] or helicity.[17] The alternative approach of constructing systems of molecules that mimic macroscopic mechanical machines presents a significant challenge in crystal engineering, as well-defined multicomponent systems are needed in which the functions of the individual molecules can be correlated with one another.

Characterizing the function and behavior of molecular machines and their components is a crucial part of their design and development. Experimentally, UV-vis spectroscopy[10,12] and increasingly, NMR,[18–26] have given insight into the molecular processes involved and their approximate rates. Because these systems and their functions are relatively well defined, they are also ideal targets for theoretical approaches, although covering the range of time scales at which they function, typically from GHz to Hz,[27] is problematic even for modern simulation techniques. The problem is exacerbated by the necessary treatment of electrons in molecular machines whose motions depend on excited state transition states or the formation of chemical bonds. Nevertheless, such systems have been tackled successfully using *ab initio* approaches, in molecular switches,[28,29] rotaxane-type molecular shuttles[10,30] and photochemically-driven, artificial cilia.[31] Where conformational properties and the stochastic behavior of molecules are solely responsible for their function, molecular dynamics (MD)[10,20,30,32–34] and molecular mechanics (MM)[31,33,35–37] are more useful and can typically obtain information on processes acting faster than 100 ns. However, even this time scale is insufficient to investigate the functionality of some of these machines. Moreover, future progress in this field will be directed towards combining many of these individual molecular components into functional molecular 'devices'. Here, it will be increasingly important to be able to fully char-

acterize correlated molecular motion so that the important design parameters can be assessed and the functionality tuned.

Our goal here has been to extend the utility of MD simulations in the aforementioned systems by demonstrating the applicability of the metadynamics algorithm in accelerating the sampling of rare events and efficiently reconstructing free energy surfaces (FESs) of complex, multidimensional processes. This very promising and increasingly popular simulation technique, first proposed by the group of Parrinello,[38] falls into the general class of umbrella sampling-type simulation techniques[39] in which the simulation trajectory is biased towards areas of interest using 'artificial', time-dependent biasing potentials. In metadynamics this potential is a function of well-defined collective variables (CVs), and is built on the fly during the simulation in such a way as to approximate the underlying FES in the space defined by those variables. Its success and increasing popularity in the literature is due not only to the efficiency of the algorithm and the acceleration it offers in both classical MD and *ab initio* approaches, but also to its versatility, as the choice of CVs that can be used is almost limitless. A wide array of CVs have been reported in the literature:[40] structural order parameters to accelerate melting,[41] clustering[42–44] and binding-type processes;[45,46] phase transitions have been induced using the simulation cell parameters as CVs;[47–49] conformational changes of molecules have been accelerated using intramolecular bond angles or order parameters for CVs,[50–52] including many studies of protein folding[53–57] and other biological processes such as ion gating[58,59] and substrate binding;[60,61] and finally, simulations of chemical reactions have been accelerated using simple internuclear vectors, basic atomic coordinates, and coordination numbers as CVs.[62–66] This versatility would clearly be a major advantage to the simulation of molecular machines, where the motions of different molecular components in a complicated system could each be represented by a separate CV in the multidimensional CV space of a single metadynamics simulation. The efficiency of the algorithm would then ensure that this complicated space was fully sampled.

To demonstrate the promise of metadynamics in the simulation of molecular machines, here we apply the algorithm to the study of the correlated molecular reorientations in the plastic crys-

tal octafluoronaphthalene (OFN); a model system which mimics a very simple molecular ratchet mechanism. In our previous studies of this material we showed that even 100 ns long molecular dynamics simulations are insufficient to sample the full rotation of the molecules, a process shown to occur by solid-state NMR.[32] Our first goal here is to show that the use of metadynamics can make the sampling of this rotation facile, confirming both the effectiveness of the method and further validating the NMR results in that study. Secondly, we extend the method to sample from the simultaneous rotational behavior of three neighboring OFN molecules, proving that they are correlated and investigating the mechanism behind the effect. Although this is a very simple model system, we hope that the success of the algorithm here will demonstrate its applicability to the study of much more complicated functional molecular machines and devices. In the following sections, a more thorough introduction to the metadynamics technique is described (including its adaptation to study rotational motion in crystals), simulation details are given, and finally results and conclusions are presented.

Methods

Metadynamics

The metadynamics algorithm[38] introduces a time-dependent bias potential, $V_{\mathrm{b}}(s,t)$ (where the quantity s is the vector of collective variables), that is used to influence and accelerate the dynamics in a predefined set of collective variables that can be calculated from a subset of the particle positions, $R(r^N)$. $V_{\mathrm{b}}(s,t)$ takes the form of a sum of Gaussian markers, with width δs and height w, centered at the values of the collective variables that have already been visited by the trajectory of the system and deposited at a time interval τ_{G};

$$V_{\mathrm{b}}(s,t) = w \sum_{t=\tau_{\mathrm{G}},2\tau_{\mathrm{G}}\ldots} \exp\left(-\frac{|s-s(t)|^2}{2\delta s^2}\right). \tag{1}$$

This potential serves to fill up the wells in the FES of the CVs. As the underlying potential is compensated for, the system escapes from local minima and can fully sample the energy surface. Once all of the states have been explored and all the wells filled, the biasing potential is expected to become a good estimate for the underlying free energy surface, $F_{\mathrm{G}}(s) = -V_{\mathrm{b}}(s, t \to \infty)$. The error associated with this estimate has been shown to depend on the metadynamics parameters w, δs and τ_{G}, as well as properties specific to the system.[67] Its origin lies in the false assertion that the estimate of the free energy obtained from the biasing potential tends towards the real, unbiased value. In fact, once the biasing potential completely compensates for $F(s)$, the addition of further Gaussian markers serves to introduce error, so that $-V_{\mathrm{b}}(s,t)$ fluctuates around the correct value of $F(s)$, with the magnitude of the fluctuations depending on the size of the markers added.

Attempts have been made to control this fluctuation,[55,68–70] the most promising of which has come from Barducci et al.[71] Here, a 'well-tempered', 'smoothly converging' form of the algorithm is proposed, in which the height of the Gaussian markers added is modified according to the relationship

$$w = \omega e^{-[V_{\mathrm{b}}(s,t)/\Delta T]} \tau_{\mathrm{G}}, \tag{2}$$

where, following the notation of Ref. 71, ω is the bias deposition rate with units of energy per unit time, $V_{\mathrm{b}}(s,t)$ is the estimate of the free energy at the current CV positions and the current time step, and ΔT is a tunable temperature-like parameter that controls how quickly w reduces as the wells are filled. In practice, ΔT also introduces a 'ceiling' to the height of $V_{\mathrm{b}}(s,t)$, which can restrict the trajectory of the CVs to lower energy regions of their phase space. In this scheme, the final value of the biasing potential is a scaled approximation to $F(s)$:

$$F(s) = -\frac{T + \Delta T}{\Delta T} V_{\mathrm{b}}(s, t \to \infty). \tag{3}$$

At the beginning of a metadynamics run using this methodology, the biasing potential is zero and so $w = \omega$, which can be quite a large value, allowing the wells to be filled quickly and leading to a rapid exploration of phase space. As the wells begin to fill up, w is scaled and progressively smaller

perturbations are made to V_b, allowing it to smoothly converge to an accurate approximation of $F(s)$. The values of ω and ΔT are chosen to achieve the best efficiency.

Collective variables for rotational motion in OFN

The key to using the metadynamics algorithm successfully lies in the choice and definition of the CVs. Here, the orientation of an individual OFN molecule is of interest and so the rotation of the molecule relative to a fixed, molecular reference frame is used as the CV. What follows in this section is a description of how this angle and its derivative are defined for the OFN molecule. However, the approach and the formulations are equally valid in other rigid molecular systems, only the definition of the molecular frame requires modification. Furthermore, multiple angles may be simultaneously biased by using a separate CV for each.

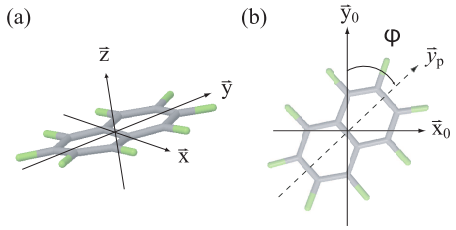

Figure 1: The molecular frame used to describe the orientation of the octafluoronaphthalene molecules. (a) The molecular axes, with the origin at the center of mass of the molecule. Vectors $\vec{x}$ and $\vec{y}$ are defined relative to collections of atoms in the molecule and $\vec{z}$ is their cross product. (b) The definition of the collective variable used, shown as the polar angle ϕ. $\vec{x_0}$ and $\vec{y_0}$ refer to the axes at time $t = 0$. Adapted from Figure 4 of Ref. 32.

The projection of the y-axis of the molecular frame onto the x_0y_0 plane, $\vec{y_p}$, was used to define the angle of rotation,

$$\vec{y_p} = \vec{z_0} \times (\vec{y_t} \times \vec{z_0}). \tag{4}$$

The collective variable is the angle ϕ between $\hat{y}_p$ (where the circumflex denotes a unit vector) at time t and its value at $t = 0$, which is equivalent to the starting vector, $\hat{y}_0$. The definition of ϕ is

thus,

$$\cos\phi = \hat{y_{\mathrm{p}}} \cdot \hat{y_0}. \tag{5}$$

This is the same angle definition as a standard valence angle with the vectors $\hat{y}_{\mathrm{p}}$ and $\hat{y}_0$ replacing the usual r_{ab} and r_{bc} bond vectors. In that case, the direction of the force that the atoms are subjected to is given by $-\frac{d\phi}{dr_l^\alpha}$, where r_l^α is the α component of the vector pointing to atom l. Here, the angle is defined in a fixed molecular frame relative to the position at $t = 0$ and so the only force direction required is that on the point, $\mathbf{P} = \mathbf{C} + \hat{y}_{\mathrm{p}}$, where $\mathbf{C}$ is the instantaneous center of mass of the molecule and thus the origin of the molecular frame. This force direction is given by,

$$f_{\mathrm{p}}^\alpha = -\frac{d\phi}{dy_{\mathrm{p}}^\alpha}, \tag{6}$$

and is perpendicular to the vector $\hat{y}_{\mathrm{p}}$while lying in the plane shared by $\hat{y}_{\mathrm{p}}$ and $\hat{y}_0$. Thus,

$$\begin{aligned} \hat{f}_{\mathrm{p}} &= |\hat{y_{\mathrm{p}}} \times (\hat{y_{\mathrm{p}}} \times \hat{y_0})| \\ &= |\hat{y_{\mathrm{p}}} \times \hat{z_0}|, \end{aligned} \tag{7}$$

using $\vec{z_0} = \vec{y_{\mathrm{p}}} \times \vec{y_0}$ which follows from the definition of the vectors and is apparent from Figure 1.

The force produces a torque on the molecule whose direction is along $\vec{z_0}$,

$$\hat{\tau}_{z_0} = \hat{y_{\mathrm{p}}} \times \hat{f}_{\mathrm{p}}. \tag{8}$$

The torque acts on the molecule as a whole, and from it the forces on individual atoms can be calculated. Remembering that as per the metadynamics algorithm, the magnitude of the force comes from the derivative of the biasing potential, $\frac{dV_{\mathrm{b}}}{ds}$, the total force on an atom, k, in the molecule is given by

$$f_{\mathrm{k}} = \frac{1}{N}\frac{dV_{\mathrm{b}}}{ds}\frac{1}{|\vec{y_{\mathrm{k}}}|}(\vec{y_{\mathrm{k}}} \times \vec{z_0}), \tag{9}$$

where $\vec{y_{\mathrm{k}}}$ is the vector pointing from the center of mass of the molecule to atom k but projected onto the x_0y_0 plane, and N is the total number of atoms in the molecule.

We have shown previously using unbiased MD simulations that the movement of OFN molecules is governed principally by their in-plane rotation,[32] the definition of which is described above. However, the molecules do have further degrees of freedom and can also tilt out of plane and roll. To further investigate the effect of the tilt, exploratory 2D metadynamics simulations were run that used the in-plane rotation and out-of-plane tilt of a single OFN molecule as CVs. The resulting FES, shown in Figure S1, demonstrates that the out of plane tilt varies in total by approximately 20–30° across the full range of in-plane orientations with the most favorable positions lying within 5–10° of the minimum energy path between the four wells. Most importantly, the FES does not have any kinks or bottlenecks that could result in significant changes in the behavior of the in-plane rotations. Therefore, although neglecting these extra degrees of freedom will affect the accuracy of the reconstructed FESs, as is discussed further in the results, the impact is expected to be limited.

Simulation details

The simulations were run using DLPOLY 2.20,[72] making use of its rigid body dynamics module to treat all of the octafluoronaphthalene molecules in the simulation cell as rigid bodies. To ensure that this treatment did not affect their rotational behavior, an unbiased 20 ns simulation was run and compared to the flexible 100 ns simulation we have reported previously.[32] The rigid 20 ns simulation, and all of the metadynamics simulations described subsequently, were run at 290 K, and use the same simulation cell as had been constructed for the 100 ns run, with 144 molecules total, corresponding to a periodic 4 x 6 x 6 arrangement along the x, y, z directions, respectively. Details of how this cell was constructed from the disordered crystal structure are given in the original reference,[32] along with the full simulation details for the 100 ns run. The modified OPLS charges and van der Waals parameters detailed in that work were also used here.

The 20 ns rigid simulation used a time step of 1 fs, with an initial equilibration period of 500 ps. The Ewald sum method was used to calculate the long-range electrostatic interactions, with the same 1.4 nm cutoff as used for the van der Waals interactions. The Nosè Hoover algorithm[73] was used to maintain constant temperature and pressure, with 1 ps relaxation times for both the barostat

and thermostat. Trajectory snapshots from every 0.5 ps of the 20 ns production run were used in the analysis.

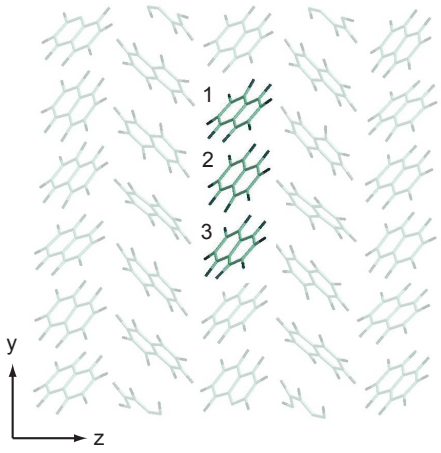

Figure 2: A slice through the *yz* plane of the OFN simulation cell illustrating the relative positions and labeling of the molecules whose orientations were used as collective variables in the 3D metadynamics simulations.

An additional metadynamics module, implementing biased rotational motion (as described above) and including both the standard and the smoothly converging form of the algorithm, was written and incorporated into the the DLPOLY 2.20 program. Simulations were run either biasing the orientation of a single molecule (1D) or simultaneously biasing the orientations of three vertically neighboring molecules (3D), as shown in Figure 2. The molecules used for metadynamics accelerated sampling were picked to be near the center of the simulation cell to simplify the analysis by avoiding any complications caused by them crossing periodic boundary conditions. The simulation parameters for the metadynamics runs matched those from the rigid 20 ns run. The reference molecular orientation used in the metadynamics calculation was taken as that of the molecule in the first simulation step, before equilibration, and therefore corresponded to the molecular orientation in the crystallographic unit cell. Values for the metadynamics parameters were estimated from examples available in the literature, with particular heed taken to the descriptions provided by Refs. 38 and 74 for the standard form of metadynamics and Ref. 71 for the smoothly converging formulation. In each case δs was limited to around 5–10° by the width of the wells in the FES as estimated from standard MD. Exploratory metadynamics runs were then used

to coarsely assess the speed and accuracy of simulations using the other parameters by comparison with the FES from standard MD. More efficient sampling was apparent when the full rotation of the molecules was observed in short (< 1ns) simulation times. For the 1D runs using the standard metadynamics algorithm (labeled MT) the biasing potential was added to every 250 MD steps ($\tau_G = 250$ fs) with wells of width, $\delta s = 5$ or 8°, and heights, $w = 0.1$ or 0.25 kJ mol^{-1} making four runs in total; the smoothly converging (labeled SC) runs all used $\delta s = 8^\circ$ and a deposition rate of $\omega = 1$ kJ mol^{-1} ps^{-1} with $\Delta T = 600$, 900 or 1200 K and $\tau_G = 100$, 250 or 500 fs, making nine runs in total. The 3D runs only used the SC form of the algorithm, again with $\delta s = 8^\circ$ and $\omega = 1$ kJ mol^{-1} ps^{-1}, and with $\Delta T = 1200$ or 1500 K and $\tau_G = 100$ or 250 fs, making four runs in total. All the metadynamics simulations were run for 10–12 ns.

Results

Comparison of rigid and flexible simulations

A comparison of the free energy profiles for the rotation of OFN molecules in the simulations using rigid and fully flexible force fields is shown in Figure 3. Here, Boltzmann inversion is used to obtain the free energy profiles directly from angle populations. Both profiles show the presence of four distinct energy wells corresponding to the four orientations adopted by the OFN molecules, labeled A–D, each of which is separated by approximately 40°. Although the extent of sampling of these wells appears to be slightly different in the two profiles, with the rigid simulation achieving better sampling of the extreme positions labeled A and D, the energy barriers to jumps between adjacent orientations remain the same. Overall, the profiles are very similar and it is clear that the use of the rigid force field does not significantly alter the rotational behavior of the molecules.

The results in Figure 3 emphasize the poor sampling that is achieved in unbiased MD simulations, as neither simulation completely explores the molecular orientations associated with the four main energy wells. This is the case even though both simulations represent a significant amount of simulation time and that the statistical averaging is performed over all 144 molecules in the

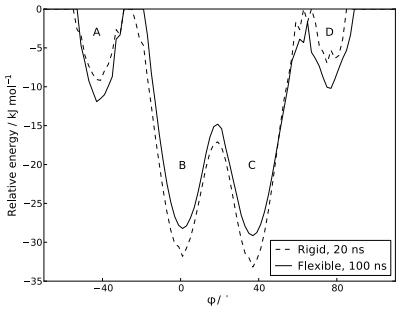

Figure 3: Comparison between the free energy profiles for the rotation of octafluoronaphthalene molecules in rigid and fully flexible simulations. An average is taken over all of the time steps and over all of the molecules in the simulation cell. Energies are defined relative to the maximum value in each free energy profile. This approach is adopted throughout to improve the clarity of the following figures. It is worth noting that the agreement between the curves would be further emphasized if the more common approach of setting the energies relative to the minimum value were used.

simulation cells. Moreover, evidence from simulations at higher temperatures (390 K) has shown that 180° rotations of the molecules are possible, but not a single example of this is seen in the ambient temperature simulations.

Metadynamics in 1D

With the initial challenge being to fully explore the energy profile for the rotation of OFN molecules at ambient temperature, metadynamics was performed using the orientation of one molecule as the only collective variable. Both the standard and smoothly converging forms of the algorithm were employed for this purpose and are directly compared for their efficacy. However, to ensure that the long runs using the standard metadynamics did not overfill the wells, the symmetry of the OFN molecules about their C_2 rotation, and hence the symmetry of the expected FES, was used to define a point at which the construction of the FES could be stopped. A parameter, χ was defined as the sum difference between 180° rotated sections of the FES,

$$\chi = \sum_{\phi=-180^\circ}^{0^\circ} |F(\phi) - F(\phi + 180^\circ)|, \tag{10}$$

and the construction of the FES halted (retrospectively) when it was at its minimum.

The reconstructed FES from a selection of the metadynamics runs are shown in Figure 4(a) alongside the unbiased simulation results presented above. The acceleration in the sampling afforded by using metadynamics is clear; the full rotational energy profiles of the molecules are sampled in very little simulation time, including the full rotation of the molecule. In fact, sampling this full rotation is facile in metadynamics and was seen in < 50 ps of simulation time in pilot runs using coarser parameters. There is quite a high degree of variation between the different runs, due to overfilling of individual wells, as is clear in the SC:500-1200 profile around well C', and due to some asymmetry in the extent of the filling in each half of the profiles. Other differences between the profiles could be caused by changes in other important degrees of freedom that are not explicitly accounted for, such as the out-of-plane tilt of the molecules, which may alter the effective FES at a given point in the simulation. These effects should average themselves out over time, but it is possible that this averaging is not complete on these surfaces with multiple energy wells, where the simulation trajectory spends relatively little time in each well.

Plotted in Figure 4(b) are profiles representing the average FESs, taken over all of the metadynamics runs for the MT and SC forms of the metadynamics algorithm. These average runs compare extremely favorably with each other, differing by no more than 2–3 kJ mol^{-1} at any given value of the collective variable, ϕ. They also follow the basic shape and magnitude of the results from the unbiased simulations, particularly in the regions where the standard MD achieves a high level of sampling, around wells B and C. The excellent agreement between the averaged FESs suggests that the slower degrees of freedom do reach an equilibrium over a time scale spanning the many simulations.

The evaluation of the barrier heights, listed in Table 1, further shows there to be a strong agreement between the different runs. The values quoted in Table 1 are estimated from the average FESs, along with the standard error from the deviation in barrier heights from all of the other metadynamics runs in each set about the average values. The barrier heights from the two different types of metadynamics runs agree with one another to within their standard error in almost every case, and the relatively low error values indicate a narrow distribution in barriers obtained from

each of the individual runs. The barrier heights from the unbiased simulations for the well-sampled jumps between wells B and C further validate the metadynamics runs, especially in their ability to distinguish the asymmetry in the jumps between B and C.

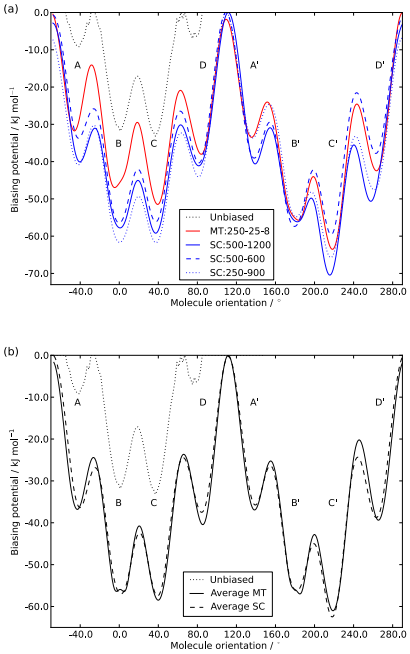

Figure 4: 1D FESs from the MT and SC metadynamics simulations, with the unbiased results displayed for comparison. (a) Results from four of the metadynamics simulations. The legend titles reflect the metadynamics parameters with the format MT:τ_G-w-δs and SC:τ_G-ΔT. (b) Average FESs from the MT and SC metadynamics runs.

It is gratifying to see that metadynamics works well for this simple case employing a single collective variable. As the reconstructed energy profiles agree very well with the minimum energy pathway recovered from the unbiased, flexible MD simulations, it is also clear that the collective variable chosen very closely traces the minimum energy path followed by the reorientation of the molecules. We note that in this case, it is also possible to apply alternative techniques such as umbrella sampling,[39] the nudged elastic band method,[75] or even newer techniques such as statistical temperature thermodynamics.[76,77]

Table 1: Barrier heights from the average histograms for the MT and SC sets of metadynamics runs. Estimates of the errors are calculated from the deviation of the energy barriers in the individual runs from those of the average histograms.

	Barrier heights / kJ mol^{-1}		
Barrier	MT	SC	Unbiased
A→D'	35.4 ± 1.9	36.8 ± 1.9	-
A→B	13.1 ± 1.7	13.4 ± 1.2	-
B→A	24.5 ± 1.4	25.5 ± 0.7	-
B→C	16.9 ± 0.8	15.5 ± 1.8	14.7
C→B	18.4 ± 2.4	16.4 ± 1.4	16.1
C→D	35.3 ± 2.5	34.0 ± 1.9	-
D→C	17.3 ± 0.4	15.5 ± 1.1	-
D→A'	40.7 ± 3.3	39.4 ± 1.6	-

Metadynamics in 3D

Previous unbiased MD results of the OFN system suggested that there may be some correlation between the orientations of the vertically neighboring molecules, with a slight preference observed for neighbors to occupy the same orientation.[32] This correlation would manifest itself in small modifications to the effective rotational FES of each individual molecule as the orientations of its neighbors change. Reliably estimating such small changes requires a very high level of sampling that would be unfeasible to achieve using unbiased MD simulations. However, as the results above suggest, the efficiency of the metadynamics algorithm should provide a route to achieve sufficient sampling to allow correlations between molecular orientations to be probed. This is done by expanding the CV space to three dimensions to simultaneously bias the orientations of three neighboring molecules. This configuration and the labeling of the three molecules is shown in Figure 2.

To minimize the complexity of this problem, which would otherwise require the complete exploration of a 3D FES with 512 energy minima (8 wells in each dimension, 8^3 in total), the calculations were modified to treat molecular orientations 180° apart from one another as being identical, allowing the CV space to be limited to a 180° span with periodic boundary conditions. This is equivalent to filling up both sides of the FES simultaneously, leaving only four energy wells

in each dimension, 64 in total.

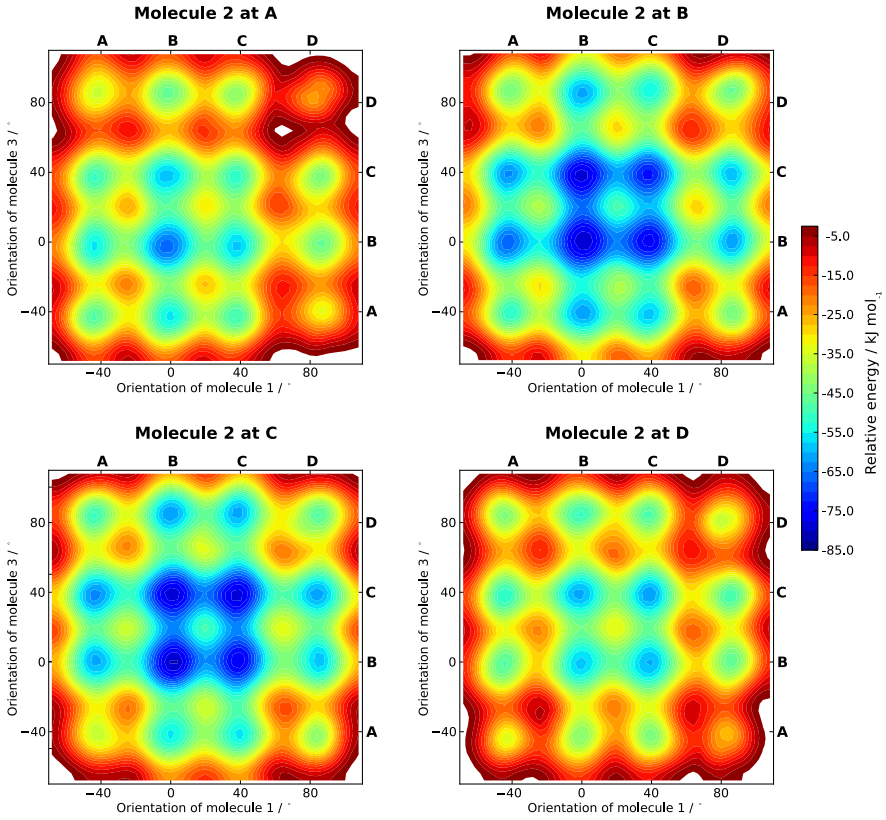

Figure 5: 2D slices taken through the 3D FES obtained from the average of the 3D metadynamics simulations. Each slice corresponds to a distinct orientation of the middle molecule, as indicated by the title above each plot.

The results from the simulations are shown in Figure 5, using the average FES of the four SC runs described in the method. Normal MT runs were not included as there was no good way to decide the stopping point of the simulations and therefore the FES would likely be overfilled. The contour plots shown are 2D slices through the 3D FES at discrete positions of the middle molecule that correspond to it sitting at the bottom of each of the four energy wells (see the individual plot titles). The plots therefore represent how the energy surface explored by the outer two molecules changes with the instantaneous orientation of the middle molecule in the stack. The basic form of each of the four surfaces demonstrates that all of the 64 wells have been explored to some extent which shows that a very high level of sampling has been achieved compared to unbiased MD simulations. Moreover, the changes in the FESs seem to be quite systematic upon the reorientation

of the middle molecule, with the regions of lowest energy in each surface tracking the orientation of molecule 2.

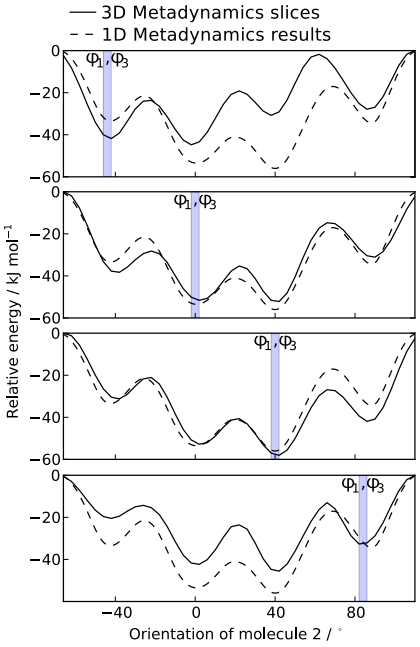

Figure 6: 1D slices taken through the average 3D FES obtained from the 3D metadynamics simulations. The slices represent 1D FESs of the middle molecule when the two other molecules are at positions corresponding to the bottom of each of the four energy wells, indicated by the gray shaded region in each plot. The average FES from the 1D SC metadynamics runs is also plotted for reference (dotted lines).

To emphasize the changes in the FES of the individual molecules upon their neighbor's reorientation, we focus on 1D slices through the energy profiles, showing the FES for the reorientation of molecule 2 (the middle molecule) when its vertical neighbors occupy discrete positions. The four slices corresponding to the points at which the two neighbors simultaneously occupy the bottom of wells A–D are shown in Figure 6, with the 1D SC metadynamics results also plotted as a reference. The plots show clearly how the orientational FES of one molecule is influenced by its neighbors' positions: the depth of the wells at and near the correlated positions become deeper, making the barriers for leaving these states slightly higher, while in most cases the barriers for jumps into these correlated positions are also reduced. All of these effects indicate a preference for the neighboring molecules to assume the same, or similar, orientations. These nearest neighbor correlations are

expected, and can be explained by the preferential charge interactions between the carbon atoms in the ring of one molecule and the fluorine atoms on the next, with the overlap between them maximized when the two neighboring molecules have the same orientation. This phenomenon is also evident in the low temperature (III) phase of octafluoronaphthalene, where the structure follows that of the dynamic, ambient temperature form but with reduced symmetry due to the motion of the molecules being frozen out. In this structure, the molecules in each stack assume the same orientation as one another, with the molecules in alternating stacks assuming the equivalent of the B and C orientations. The occupation of the B and C orientations at low temperatures is unsurprising as they are shown to be the lowest energy orientations in the FES, while the preference for the molecular orientations to order within each stack confirms the favorable energetics associated with the correlated orientations.

To investigate these effects further, the methodology described here could be extended by developing a metadynamics collective variable that includes and accelerates the sampling of the orientations of all of the molecules in the cell simultaneously. Although outside of the scope of the current work and its applications to exploring the varied interactions in molecular machines, this approach would yield further insight into the correlated motions of molecules in a whole simulation cell and would be a general approach to investigate phase transitions in molecular crystals and other homogeneous, dynamic solids.

Although the form of the motion of individual molecules is quite simple and accessible to unbiased MD at elevated temperatures, the extent of the sampling required to fill the large, complicated, 3D space defined here rules out the use of standard MD. The use of metadynamics has allowed the energy surface to be explored fully, and accurately enough to show subtle differences in molecular behavior as the local environment of the molecules changes. Specifically, as its neighbor rotates into a new position, the rotational energy profile of a molecule is modified so as to favor a rotation towards the orientation of that neighbor. This effect would be difficult to observe experimentally by either NMR or diffraction measurements, but is confirmed by the biased simulations presented here and corroborated by the low temperature behavior of the material.

Conclusions

We have demonstrated the utility of the metadynamics algorithm in exploring the free energy surface defining the motional degrees of freedom of a system of interacting molecules, using the plastic crystal, octafluoronaphthalene as a test system. This compound contains stacks of individually rotating molecules that can assume discrete orientations. It has been shown that applying the metadynamics algorithm with a single molecular orientation as the collective variable allows the full and accurate exploration of the orientational FES for the individual OFN molecules in very short simulation time (< 50 ps), a feat that was not possible in 100 ns of unbiased simulations at the same temperature. By expanding the approach and assigning the orientation of three neighboring OFN molecules as separate collective variables it has also been possible to explore the effect of correlations between them and observe how the effective rotational energy profile of a given molecule changes depending on the orientations of its closest neighbors. This required the accurate determination of a 3D free energy surface with a complicated topology, which would not have been possible using unbiased molecular dynamics simulation.

Although resembling a mechanical cog and ratchet system in its form, the overall functionality of this set of interacting molecules in the octafluoronaphthalene crystal is limited. However, the techniques applied in this study are highly suited to the evaluation of the correlated motions of molecular degrees of freedom in crystalline systems, as will be desired in engineered, crystalline molecular machines, where it would be possible to account for each degree of freedom in a given molecular machine as a separate collective variable so that the full energy surface for the machine's function can be reconstructed. The vast reduction in computational cost should also make elaborate analyses more feasible.

Supporting Information

A plot of the 2D FES explored by the in-plane rotation and out-of-plane tilt of a single OFN molecule, as estimated by a 2D smoothly converging metadynamics run using these quantities as

CVs. This material is available free of charge via the Internet at http://pubs.acs.org

Acknowledgement

S.P. was supported under EPSRC grant EP/D055237/1. A.J.I. was supported through the EPRSC Doctoral Training Account scheme. The authors wish to thank Durham University for computer time on the Hamilton high performance computer system. The authors declare no competing financial interest.

References

[1] Hess, H.; Bachand, G. Biomolecular Motors. *Mater. Today* **2005**, *8*, 22–29.

[2] Berg, H. The Rotary Motor of Bacterial Flagella. *Biochemistry* **2003**, *72*, 19.

[3] Yonekura, K.; Maki-Yonekura, S.; Namba, K. Complete Atomic Model of the Bacterial Flagellar Filament by Electron Cryomicroscopy. *Nature* **2003**, *424*, 643–650.

[4] Mayans, O.; Van der Ven, P.; Wilm, M.; Mues, A.; Young, P.; Fürst, D.; Wilmanns, M.; Gautel, M. Structural Basis for Activation of the Titin Kinase Domain during Myofibrillogenesis. *Nature* **1998**, *395*, 863–870.

[5] Iwamura, H.; Mislow, K. Stereochemical Consequences of Dynamic Gearing. *Acc. Chem. Res.* **1988**, *21*, 175–182.

[6] Bedard, T. C.; Moore, J. S. Design and Synthesis of Molecular Turnstiles. *J. Am. Chem. Soc.* **1995**, *117*, 10662–10671.

[7] Godinez, C. E.; Zepeda, G.; Mortko, C. J.; Dang, H.; Garcia-Garibay, M. A. Molecular Crystals with Moving Parts: Synthesis, Characterization, and Crystal Packing of Molecular Gyroscopes with Methyl-Substituted Triptycyl Frames. *J. Org. Chem.* **2004**, *69*, 1652–1662.

[8] Rodriguez-Molina, B.; Ochoa, M.; Farfán, N.; Santillan, R.; García-Garibay, M. Synthesis, Characterization, and Rotational Dynamics of Crystalline Molecular Compasses with N-Heterocyclic Rotators. *J. Org. Chem.* **2009**, *74*, 8554–8565.

[9] Kullmann, M.; Ruetzel, S.; Buback, J.; Nuernberger, P.; Brixner, T. Reaction Dynamics of a Molecular Switch Unveiled by Coherent Two-Dimensional Electronic Spectroscopy. *J. Am. Chem. Soc.* **2011**, *133*, 13074–13080.

[10] Mancini, G.; Zazza, C.; Aschi, M.; Sanna, N. Conformational Analysis and UV/Vis Spectroscopic Properties of a Rotaxane-Based Molecular Machine in Acetonitrile Dilute Solution: When Simulations Meet Experiments. *Phys. Chem. Chem. Phys.* **2011**, *13*, 2342.

[11] Feringa, B. L.; van Delden, R. A.; Koumura, N.; Geertsema, E. M. Chiroptical Molecular Switches. *Chem. Rev.* **2000**, *100*, 1789–1816.

[12] Klok, M.; Boyle, N.; Pryce, M. T.; Meetsma, A.; Browne, W. R.; Feringa, B. L. MHz Unidirectional Rotation of Molecular Rotary Motors. *J. Am. Chem. Soc.* **2008**, *130*, 10484–10485.

[13] Shirai, Y.; Morin, J.-F.; Sasaki, T.; Guerrero, J. M.; Tour, J. M. Recent Progress on Nanovehicles. *Chem. Soc. Rev.* **2006**, *35*, 1043.

[14] Khuong, T. A. V.; Nunez, J. E.; Godinez, C. E.; Garcia-Garibay, M. A. Crystalline Molecular Machines: A Quest Toward Solid-State Dynamics and Function. *Acc. Chem. Res.* **2006**, *39*, 413–422.

[15] Garcia-Garibay, M. A. Crystalline Molecular Machines: Encoding Supramolecular Dynamics into Molecular Structure. *Proc. Natl. Acad. Sci. U.S.A.* **2005**, *102*, 10771.

[16] van Delden, R.; Koumura, N.; Harada, N.; Feringa, B. Unidirectional Rotary Motion in a Liquid Crystalline Environment: Color Tuning by a Molecular Motor. *Proc. Natl. Acad. Sci. U.S.A.* **2002**, *99*, 4945–4949.

[17] Pijper, D.; Jongejan, M.; Meetsma, A.; Feringa, B. Light-Controlled Supramolecular Helicity of a Liquid Crystalline Phase using a Helical Polymer Functionalized with a Single Chiroptical Molecular Switch. *J. Am. Chem. Soc.* **2008**, *130*, 4541–4552.

[18] Dominguez, Z.; Khuong, T. A. V.; Dang, H.; Sanrame, C. N.; Nuñez, J. E.; Garcia-Garibay, M. A. Molecular Compasses and Gyroscopes with Polar Rotors: Synthesis and Characterization of Crystalline Forms. *J. Am. Chem. Soc.* **2003**, *125*, 8827–8837.

[19] Kottas, G. S.; Clarke, L. I.; Horinek, D.; Michl, J. Artificial Molecular Rotors. *Chem. Rev.* **2005**, *105*, 1281–1376.

[20] Albunia, A. R.; Gaeta, C.; Neri, P.; Grassi, A.; Milano, G. Dynamics of Benzene Guest Inside a Self-Assembled Cylindrical Capsule: A Combined Solid-State 2H NMR and Molecular Dynamics Simulation Study. *J. Phys. Chem. B* **2006**, *110*, 19207–19214.

[21] Garcia-Garibay, M. A.; Godinez, C. E. Engineering Crystal Packing and Internal Dynamics in Molecular Gyroscopes by Refining their Components. Fast Exchange of a Phenylene Rotator by 2H NMR. *Cryst. Growth Des.* **2009**, *9*, 3124–3128.

[22] Karlen, S. D.; Reyes, H.; Taylor, R. E.; Khan, S. I.; Hawthorne, M. F.; Garcia-Garibay, M. A. Symmetry and Dynamics of Molecular Rotors in Amphidynamic Molecular Crystals. *Proc. Natl. Acad. Sci. U.S.A.* **2010**, *107*, 14973–14977.

[23] Rodríguez-Molina, B.; Farfán, N.; Romero, M.; Méndez-Stivalet, J. M.; Santillan, R.; Garcia-Garibay, M. A. Anisochronous Dynamics in a Crystalline Array of Steroidal Molecular Rotors: Evidence of Correlated Motion within 1D Helical Domains. *J. Am. Chem. Soc.* **2011**, *133*, 7280–7283.

[24] O'Brien, Z. J.; Natarajan, A.; Khan, S.; Garcia-Garibay, M. A. Synthesis and Solid-State Rotational Dynamics of Molecular Gyroscopes with a Robust and Low Density Structure Built with a Phenylene Rotator and a Tri(*meta*-terphenyl)methyl Stator. *Cryst. Growth Des.* **2011**, *11*, 2654–2659.

[25] Hodgkinson, P. In *NMR Crystallography*; Harris, R. K., Wasylishen, R. E., Duer, M. J., Eds.; EMR Handbooks; John Wiley & Sons, Chichester, 2009; Chapter Intramolecular Motion in Crystalline Organic Solids, pp 375–386.

[26] Apperley, D. C.; Harris, R. K.; Hodgkinson, P. *Solid-State NMR: Basic Principles and Practice*; Momentum Press: New York, 2012.

[27] Khoung, T. A. V.; Nunez, J. E.; Godinez, C. E.; Garcia-Garibay, M. A. Crystalline Molecular Machines: A Quest Toward Solid-State Dynamics and Function. *Acc. Chem. Res.* **2006**, 413–422.

[28] Carstensen, O.; Sielk, J.; Schönborn, J. B.; Granucci, G.; Hartke, B. Unusual Photochemical Dynamics of a Bridged Azobenzene Derivative. *J. Chem. Phys.* **2010**, *133*, 124305.

[29] Shumkin, G. N.; Popov, A. M.; Curioni, A.; Laino, T. Ab Initio Simulation of a Molecular Switch on the Base of an Isomerization Reaction. *Math. Models Comput. Simul.* **2011**, *3*, 375–381.

[30] Zazza, C.; Mancini, G.; Brancato, G.; Sanna, N.; Barone, V. Neutral Molecular Shuttle in Acetonitrile Dilute Solution Investigated by Molecular Dynamics and Density Functional Theory. *Comput. Theor. Chem.* **2012**, *985*, 53–61.

[31] Raeker, T.; Carstensen, N. O.; Hartke, B. Simulating a Molecular Machine in Action. *J. Phys. Chem. A* **2012**, 120904145905007.

[32] Ilott, A. J.; Palucha, S.; Batsanov, A. S.; Wilson, M. R.; Hodgkinson, P. Elucidation of Structure and Dynamics in Solid Octafluoronaphthalene from Combined NMR, Diffraction, And Molecular Dynamics Studies. *J. Am. Chem. Soc.* **2010**, *132*, 5179–5185.

[33] Grabuleda, X.; Jaime, C. Molecular Shuttles. A Computational Study (MM and MD) on the Translational Isomerism in Some [2]Rotaxanes. *J. Org. Chem.* **1998**, *63*, 9635–9643.

[34] Zhang, Q.; Tu, Y.; Tian, H.; Zhao, Y.-L.; Stoddart, J. F.; Ågren, H. Working Mechanism for a Redox Switchable Molecular Machine Based on Cyclodextrin: A Free Energy Profile Approach. *J. Phys. Chem. B* **2010**, *114*, 6561–6566.

[35] Zimmerman, H. E.; Zhu, Z. General Predictor for Photoreactivity in Crystal Lattices: Molecular Mechanics in Crystalline Media and Lock and Key Control. Reaction Examples. *J. Am. Chem. Soc.* **1994**, *116*, 9757–9758.

[36] Jarowski, P. D.; Houk, K. N.; Garcia-Garibay, M. A. Importance of Correlated Motions on the Low Barrier Rotational Potentials of Crystalline Molecular Gyroscopes. *J. Am. Chem. Soc.* **2007**, *129*, 3110–3117.

[37] Deleuze, M. S.; Leigh, D. A.; Zerbetto, F. How Do Benzylic Amide [2]Catenane Rings Rotate? *J. Am. Chem. Soc.* **1999**, *121*, 2364–2379.

[38] Laio, A.; Parrinello, M. Escaping Free-Energy Minima. *Proc. Natl. Acad. Sci. U. S. A.* **2002**, *99*, 12562.

[39] Torrie, G. M.; Valleau, J. P. Monte Carlo Free Energy Estimates using Non-Boltzmann Sampling: Application to the Sub-Critical Lennard-Jones Fluid. *Chem. Phys. Lett.* **1974**, *28*, 578–581.

[40] Barducci, A.; Bonomi, M.; Parrinello, M. Metadynamics. *Wiley Interdiscip. Rev.: Comput. Mol. Sci.* **2011**, *1*, 826–843.

[41] Donadio, D.; Raiteri, P.; Parrinello, M. Topological Defects and Bulk Melting of Hexagonal Ice. *J. Phys. Chem. B* **2005**, *109*, 5421–5424.

[42] Quigley, D.; Rodger, P. M. Metadynamics Simulations of Ice Nucleation and Growth. *J. Chem. Phys.* **2008**, *128*, 154518.

[43] Santarossa, G.; Vargas, A.; Iannuzzi, M.; Baiker, A. Free Energy Surface of Two- and Three-Dimensional Transitions of Au 12 Nanoclusters Obtained by ab Initio Metadynamics. *Phys. Rev. B* **2010**, *81*, 174205.

[44] Zhai, Y.; Laio, A.; Tosatti, E.; Gong, X.-G. Finite Temperature Properties of Clusters by Replica Exchange Metadynamics: The Water Nonamer. *J. Am. Chem. Soc.* **2011**, *133*, 2535–2540.

[45] Tribello, G. A.; Liew, C.; Parrinello, M. Binding of Calcium and Carbonate to Polyacrylates. *J. Phys. Chem. B* **2009**, *113*, 7081–7085.

[46] Pietrucci, F.; Gerra, G.; Andreoni, W. CdTe Surfaces: Characterizing Dynamical Processes with First-Principles Metadynamics. *Appl. Phys. Lett.* **2010**, *97*, 141914.

[47] Sun, J.; Klug, D. D.; Martovnák, R.; Montoya, J. A.; Lee, M. S.; Scandolo, S.; Tosatti, E. High-Pressure Polymeric Phases of Carbon Dioxide. *Proc. Natl. Acad. Sci. U. S. A.* **2009**, *106*, 6077.

[48] Martoňák, R.; Laio, A.; Parrinello, M. Predicting Crystal Structures: The Parrinello-Rahman Method Revisited. *Phys. Rev. Lett.* **2003**, *90*, 75503.

[49] Pagliai, M.; Iannuzzi, M.; Cardini, G.; Parrinello, M.; Schettino, V. Lithium Hydroxide Phase Transition under High Pressure: An ab Initio Molecular Dynamics Study. *ChemPhysChem* **2006**, *7*, 141–147.

[50] Spiwok, V.; Lipovová, P.; Králová, B. Metadynamics in Essential Coordinates: Free Energy Simulation of Conformational Changes. *J. Phys. Chem. B* **2007**, *111*, 3073–3076.

[51] Donadio, D.; Bernasconi, M. Ab Initio Simulation of Photoinduced Transformation of Small Rings in Amorphous Silica. *Phys. Rev. B* **2005**, *71*.

[52] Barducci, A.; Bonomi, M.; Parrinello, M. Linking Well-Tempered Metadynamics Simulations with Experiments. *Biophys. J.* **2010**, *98*, L44–L46.

[53] Bussi, G.; Gervasio, F. L.; Laio, A.; Parrinello, M. Free-Energy Landscape for β Hairpin Folding from Combined Parallel Tempering and Metadynamics. *J. Am. Chem. Soc.* **2006**, *128*, 13435–13441.

[54] Piana, S.; Laio, A. A Bias-Exchange Approach to Protein Folding. *J. Phys. Chem. B* **2007**, *111*, 4553–4559.

[55] Babin, V.; Roland, C.; Darden, T. A.; Sagui, C. The Free Energy Landscape of Small Peptides as Obtained from Metadynamics with Umbrella Sampling Corrections. *J. Chem. Phys.* **2006**, *125*, 204909.

[56] Prakash, M. K.; Barducci, A.; Parrinello, M. Probing the Mechanism of pH-Induced Large-Scale Conformational Changes in Dengue Virus Envelope Protein Using Atomistic Simulations. *Biophys. J.* **2010**, *99*, 588–594.

[57] Cossio, P.; Marinelli, F.; Laio, A.; Pietrucci, F. Optimizing the Performance of Bias-Exchange Metadynamics: Folding a 48-Residue LysM Domain Using a Coarse-Grained Model. *J. Phys. Chem. B* **2010**, *114*, 3259–3265.

[58] Gervasio, F. L.; Parrinello, M.; Ceccarelli, M.; Klein, M. L. Exploring the Gating Mechanism in the ClC Chloride Channel via Metadynamics. *J. Mol. Biol.* **2006**, *361*, 390–398.

[59] Piccinini, E.; Ceccarelli, M.; Affinito, F.; Brunetti, R.; Jacoboni, C. Biased Molecular Simulations for Free-Energy Mapping: A Comparison on the KcsA Channel as a Test Case. *J. Chem. Theory Comput.* **2008**, *4*, 173–183.

[60] Grazioso, G.; Limongelli, V.; Branduardi, D.; Novellino, E.; De Micheli, C.; Cavalli, A.; Parrinello, M. Investigating the Mechanism of Substrate Uptake and Release in the Glutamate Transporter Homologue GltPh through Metadynamics Simulations. *J. Am. Chem. Soc.* **2012**, *134*, 453–463.

[61] Biarnés, X.; Bongarzone, S.; Vargiu, A. V.; Carloni, P.; Ruggerone, P. Molecular Motions in Drug Design: the Coming Age of the Metadynamics Method. *J. Comput. Aided Mol. Des.* **2011**, *25*, 395–402.

[62] Stirling, A.; Iannuzzi, M.; Parrinello, M.; Molnar, F.; Bernhart, V.; Luinstra, G. A. β-Lactone Synthesis from Epoxide and CO: Reaction Mechanism Revisited. *Organometallics* **2005**, *24*, 2533–2537.

[63] Ensing, B.; Klein, M. L. Perspective on the Reactions Between F– and CH3CH2F: The Free Energy Landscape of the E2 and SN2 Reaction Channels. *Proc. Natl. Acad. Sci. U. S. A.* **2005**, *102*, 6755.

[64] Blumberger, J.; Ensing, B.; Klein, M. Formamide Hydrolysis in Alkaline Aqueous Solution: Insight from ab Initio Metadynamics Calculations. *Angew. Chem. Int. Ed.* **2006**, *45*, 2893–2897.

[65] Cucinotta, C. S.; Ruini, A.; Catellani, A.; Stirling, A. Ab Initio Exploration of Rearrangement Reactions: Intramolecular Hydrogen Scrambling Processes in Acetone. *J. Phys. Chem. A* **2006**, *110*, 14013–14017.

[66] Ceriotti, M.; Cereda, S.; Montalenti, F.; Miglio, L.; Bernasconi, M. Ab Initio Study of the Diffusion and Decomposition Pathways of SiHx Species on Si(100). *Phys. Rev. B* **2009**, *79*.

[67] Laio, A.; Rodriguez-Fortea, A.; Gervasio, F. L.; Ceccarelli, M.; Parrinello, M. Assessing the Accuracy of Metadynamics. *J. Phys. Chem. B* **2005**, *109*, 6714–6721.

[68] Wu, Y.; Schmitt, J. D.; Car, R. Mapping Potential Energy Surfaces. *J. Chem. Phys.* **2004**, *121*, 1193.

[69] Micheletti, C.; Laio, A.; Parrinello, M. Reconstructing the Density of States by History-Dependent Metadynamics. *Phys. Rev. Lett.* **2004**, *92*, 170601.

[70] Min, D.; Liu, Y.; Carbone, I.; Yang, W. On the Convergence Improvement in the Metadynamics Simulations: A Wang-Landau Recursion Approach. *J. Chem. Phys.* **2007**, *126*, 194104.

[71] Barducci, A.; Bussi, G.; Parrinello, M. Well-Tempered Metadynamics: A Smoothly Converging and Tunable Free-Energy Method. *Phys. Rev. Lett.* **2008**, *100*, 20603.

[72] Smith, W.; Forester, T. DL_POLY_2.0: A General-Purpose Parallel Molecular Dynamics Simulation Package. *J. Mol. Graphics* **1996**, *14*, 136.

[73] Hoover, W. G. Canonical Dynamics: Equilibrium Phase-Space Distributions. *Phys. Rev. A* **1985**, *31*, 1695–1697.

[74] Laio, A.; Gervasio, F. Metadynamics: A Method to Simulate Rare Events and Reconstruct the Free Energy in Biophysics, Chemistry and Material Science. *Rep. Prog. Phys.* **2008**, *71*, 126601.

[75] Jønsson, H.; Mills, G.; Jacobsen, K. Nudged Elastic Band Method for Finding Minimum Energy Paths of Transitions. In *Classical and Quantum Dynamics in Condensed Phase Simulations;* Berne, B. J., Ciccotti, G. and Coker, D. F. Eds.; World Scientific: Singapore. 1998.

[76] Kim, J.; Straub, J.; Keyes, T. Statistical-Temperature Monte Carlo and Molecular Dynamics Algorithms. *Phys. Rev. Lett.* **2006**, *97*, 050601.

[77] Lintuvuori, J.; Wilson, M. Statistical Temperature Molecular Dynamics Simulations Applied to Phase Transitions in Liquid Crystalline Systems. *J. Chem. Phys.* **2010**, *132*, 224902.